Solar Energy 159 (2018) 834–840

Contents lists available at ScienceDirect

Solar Energy

journal homepage: www.elsevier.com/locate/solener

Characterisation of SnSe thin films fabricated by chemical molecular beam deposition for use in thin film solar cells

T.M. Razykov[a,*], G.S. Boltaev[b], A. Bosio[c], B. Ergashev[a], K.M. Kouchkarov[a], N.K. Mamarasulov[a], A.A. Mavlonov[a], A. Romeo[d], N. Romeo[c], O.M. Tursunkulov[e], R. Yuldoshov[a]

[a] Physical-Technical Institute, Uzbekistan Academy of Sciences, Bodomzor Yoli 2"B", Tashkent 100084, Uzbekistan
[b] Ion-Plasma and Laser Technologies, Uzbek Academy of Sciences, Tashkent 100125, Uzbekistan
[c] University of Parma, G.P Usberti 7/A, 43124 Parma, Italy
[d] Universita' di Verona, Ca' Vignal 2- Strada Le Grazie 15, 37134 Verona, Italy
[e] Educational-Experimental Centre of High Technology, Talabalar Shaharchasi 3A, Tashkent 100174, Uzbekistan

ARTICLE INFO

Keywords:
Thin film
SnSe
Chemical molecular beam deposition
Bandgap

ABSTRACT

SnSe thin films were fabricated the first time by chemical molecular beam deposition (CMBD) in atmospheric pressure hydrogen flow using polycrystalline tin selenium (SnSe) precursors. The morphological and electrical properties of the films were studied as a function of the precursor's composition and the substrate temperature. Experimental data indicate that in the resulting thin films Se enrichment takes place at low substrate temperatures, despite the different compositions of the SnSe precursor during the synthesis. In this case, the grain sizes of the films vary in the range of (8–20) μm, depending on the substrate temperature. In addition, X-ray diffraction analysis of the samples shows that the films have an orthorhombic crystalline structure. The electrical conductivity of films measured by van der Pauw method varies between 6 and 90 $(\Omega \times \mathrm{cm})^{-1}$. The optical measurements on selected SnSe thin films illustrate that the samples have an optical bandgap of (1.1–1.2) eV and the absorption coefficient of $\sim 10^5\,\mathrm{cm}^{-1}$, which is suitable for thin film solar cells.

1. Introduction

Currently, the leading material in the world photovoltaic (PV) market is wafer-based silicon (Si) with an efficiency of 26.3% (Yoshikawa et al., 2017). However, approximately 50% of the cost of the finished Si solar cells is due to the expensive fabrication processes of Si wafers, whereas thin-film solar cells are considered to be less expensive alternatives compared to the wafer-based Si solar cells (Hamakawa, 2004; Vallat-Sauvain et al., 2006; Razykov et al., 2011). During the last two decades, $Cu(In,Ga)Se_2$ (CIGSe) and CdTe based solar cells have reached high conversion efficiency of 22.6% (Jackson et al., 2016) and 22.1% (Green et al., 2016), respectively. Although with these high efficiencies, further large-scale applications for thin-film solar cells based on CIGSe and CdTe materials are also complicated because of the limited In, Ga, Te in the earth's crust, as well as the toxicity issues of Cd (Dhere, 2011).

Proceeding from this, many research centres and laboratories have aimed to replace these expensive materials of In and Ga with Zn and Sn elements in CIGSe as the main optical properties of these materials are suggested to be unaffected. The main advantages of these elements are their low cost (prevalence in nature) and non-toxicity. To date, the efficiency of solar cells based on $Cu_2ZnSnS_xSe_{4-x}$ (CZTSe) is 12.6%. So far, this data was obtained in IBM's research center and is the maximum for the last 20 years (Wang et al., 2013). As CZTSSe belongs to a quaternary system, the precise control of composition and structural transitions is difficult due to more number of elements (Jung et al., 2017; Todorov et al., 2013). Moreover, too many elements in this absorber may also increase the production cost of the solar cells. Therefore, in view of mass production at lower cost, the use of both CIGSe and CZTSe will be limited in the near future.

Tin-based binary semiconductors, such as SnS and SnSe are expected to play a crucial role in replacing the above technologies in the near future owing to their relatively earth-abundance, non-toxic nature, and easy controllability of stoichiometry (Banu et al., 2017; Jeong et al., 2017; Kawano et al., 2016; Zakutayev, 2017).

These materials exhibit favorable properties, such as high chemical stability, suitable bandgap of (1.0–1.5) eV and high absorption coefficient ($\sim 10^5\,\mathrm{cm}^{-1}$) with *p*-type conductivity (Boscher et al., 2008; Indirajith et al., 2010; Kumar et al., 2015; Mathews, 2012; Reddy et al., 2016; Suguna et al., 1996,). In addition, they show a maximum

* Corresponding author.
E-mail address: razykov@uzsci.net (T.M. Razykov).

https://doi.org/10.1016/j.solener.2017.11.053
Received 12 October 2017; Received in revised form 11 November 2017; Accepted 20 November 2017

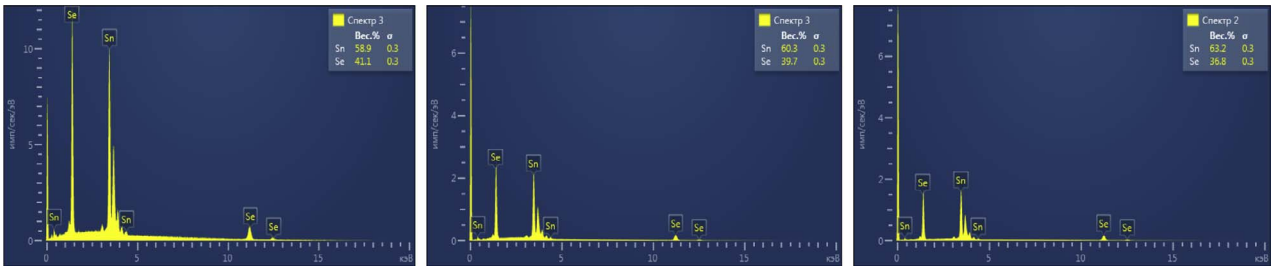

$Sn_{0.55}Se_{0.45}$ T=720 K $Sn_{0.5}Se_{0.5}$ T=770 K $Sn_{0.55}Se_{0.45}$ T=820 K

Fig. 1. Results of energy dispersive X-ray spectroscopy analysis for SnSe thin films deposited from Sn enriched precursor at indicated substrate temperatures.

theoretical efficiency of 32% (Reddy et al., 2016). Therefore, these materials have great potential to replace the toxic (CdTe) and scarce elements based (CIGS) absorbers in photovoltaic devices. On the other hand, the solar cells fabricated from these materials (SnS and SnSe) currently exhibited lower efficiencies ($\leq$1% by non-vacuum methods and $<$ 5% by vacuum methods) than CIGS and CZTS solar cells. The lower efficiency has been attributed to a lack of precise control over the pure phase formation and fine-tuning of the bandgap by the adopted technology. In thermal growth methods, owing to high volatility of sulfur, it is very difficult to maintain the 1:1 ratio of Sn:S (Wakeham and Hawkins, 2006). The sulfur deficiency can lead to the tin migration to grain boundaries, surfaces, interfaces, interstitial sites, or sulfur antisites (Wakeham and Hawkins, 2006). In addition, the problem of a good heterojunction partner has not been fully rectified. All aforementioned issues can strongly influence the recombination losses at the device level (Wakeham and Hawkins, 2006).

To obtain SnSe thin films, various growth methods such as thermal evaporation (Indirajith et al., 2010), chemical vapor deposition (Boscher et al., 2008; Suguna et al., 1996) electrodeposition (Mathews, 2012), spray pyrolisis (Martínez-Escobar et al., 2013), magnetron sputtering (Wakeham and Hawkins, 2006) and others are used. The physical characteristics of the films, i.e. the optical bandgap, the direction and degree of preferential growth orientation, the elemental composition, strongly depend on the growth conditions. In most cases, additional heat treatment (post-annealing) is required to obtain the resulting films with the optimal characteristics for their effective usage in thin-film solar cells.

The purpose of this work is to obtain SnSe thin films by technologically simple CMBD method and study their physical properties as a function of growth conditions for photovoltaic application.

2. Experimental

Polycrystalline SnSe precursors with the following proportions were used as source materials: (1) Sn-50 wt% and Se-50 wt%; (2) Sn-50.7 wt % and Se 49.3 wt%; (3) Sn-40 wt% and Se-60 wt%. The SnSe precursors were obtained as follows: the Sn and Se elements were placed in quartz ampoules in which a vacuum was created. Subsequently, quartz ampoules were loaded into a furnace and heated at 1150 K for 72 h in order to synthesize SnSe compounds. Finally, quartz ampoules were cooled to room temperature (RT). In order to check whether SnSe compounds were formed, X-ray diffraction (XRD) measurements were performed. XRD analysis shows that SnSe compounds were formed which have an orthorhombic crystal structure.

The preparation of a polycrystalline SnSe thin film was carried out according to the procedure described in (Razykov, 1991). The evaporator was loaded with SnSe precursor and it was put into the growth chamber and purged with hydrogen in order to remove atmospheric pollutants from it. Subsequently, the outer furnace of the chamber was turned on. The heating level is determined by the set deposition temperatures. When the substrate has reached the required temperature, the individual heater is turned on in order to adjust the evaporator temperature to the required temperature. The temperature of evaporation was established to be in the range of (1120–1220) K, and the temperature of the substrate was varied between (720–770) K. Hydrogen was used as carrier gas with a flow rate of ~20 cm^3/min. The duration of the deposition process depends on the required film thickness and ranges between (30 and 60) min. All SnSe thin films have been grown on (40 × 40) mm^2 in size borosilicate glasses. Subsequently, these samples were cut into (10 × 10) mm^2 pieces in order to investigate their physical properties.

The crystal structure and the phase of the material compositions were studied by XRD using a “Panalytical Empyrean” diffractometer (CuKα radiation, λ = 1.5418 Å) with a wide-angle measurements of 2θ in the range of (20–80)° and a step of 0.01°. The experimental data were analyzed using the Joint Committee on Powder Diffraction Standard (JCPDS). Morphological studies were carried out using a scanning electron microscope (SEM-EVO MA 10), and film compositions were determined using an energy-dispersive X-ray spectroscopy (EDX, Oxford Instrument - Aztec Energy Advanced X-act SDD).

Optical parameters of selected SnSe thin films were determined from the transmission spectra obtained in a wide spectral range between (400 and 2500) nm using the HR 4000 Ocean Optic spectrometer with a resolution of 2 nm.

For electrical measurements, ohmic contacts were realized by vacuum deposition of metals on as-deposited films. Silver was used as an ohmic contact. The type of conductivity of the samples was determined by thermoelectric effect. The electrical conductivity of films, i.e. along the lateral direction, were measured by van der Pauw method. The thickness of the films (1–3) μm was determined using microinterferometer MII-4, and the method of precision micro-weighting (on FA 120 4C scales with an accuracy of 0.1 mg).

Table 1
Results of energy dispersive X-ray spectroscopy analysis for SnSe thin films deposited from Se enriched and stoichiometric SnSe precursors. T_s is the substrate temperature.

T_s (K)	SnSe thin films deposited from stoichiometric SnSe precursor			SnSe thin films deposited from Se enriched SnSe precursor		
	Composition of the film	Sn, wt.%	Se, wt. %	Composition of the film	Sn, wt.%	Se, wt. %
720	$Sn_{0.48}Se_{0.52}$	57.8	42.2	$Sn_{0.48}Se_{0.52}$	57.3	42.7
770	$Sn_{0.48}Se_{0.52}$	57.8	42.2	$Sn_{0.49}Se_{0.51}$	59.2	40.8
820	$Sn_{0.49}Se_{0.51}$	58.2	41.8	$Sn_{0.49}Se_{0.51}$	58.7	41.3

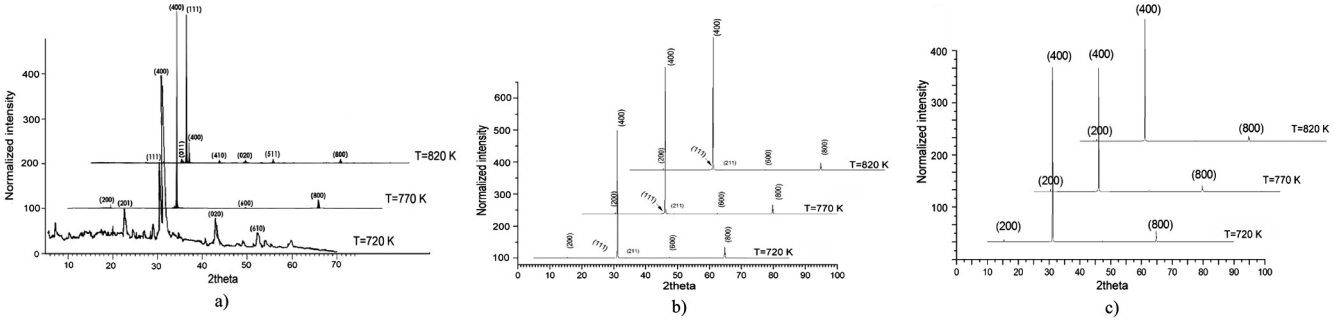

Fig. 2. Wide-angle X-ray spectra of SnSe films obtained from (a) Sn enriched, (b) stoichiometric and (c) Se enriched SnSe precursors at three different substrate temperatures.

3. Results and discussion

According to EDX data, the obtained films do not have any impurity elements within the sensitivity of the method (cf. Fig. 1). The deposited films from the Sn enriched SnSe precursor have an almost similar, stoichiometric composition at substrate temperatures of 720 K and 770 K. On the other hand, the film grown at 820 K has Sn enriched composition. This might be explained by the fact that when the substrate temperature increases, Se re-evaporates from the substrate, which results in enrichment of the Sn in the films as this effect was observed in CdSe thin films (Razykov and Kuchkarov, 2004). All films deposited from the SnSe precursors enriched with Se and stoichiometric composition, yielded Se enriched composition in the films at different temperatures (cf. Table 1). All SnSe films studied in this work have a smooth surface without cracks and pores on the surface of the substrate. Thermoelectric studies depict that all SnSe films exhibit a *p*-type conductivity.

Fig. 2 shows the XRD patterns of SnSe films deposited from three different SnSe precursors, i.e. Sn enriched, Se enriched and with stoichiometric composition, for three different substrate temperatures. According to XRD analysis, all thin films showed single-phase, the orthorhombic structure of SnSe and there are no other crystalline phases of Sn, Se, Sn_2Se_3, $SnSe_2$, SnO_2, etc. As depicted, the main peaks are corresponding to the (4 0 0) and (1 1 1) preferential orientation of SnSe. A similar results were also noted in several works devoted to SnSe films obtained by thermal evaporation and chemical vapor deposition (Boscher et al., 2008; Indirajith et al., 2010). The authors ascribe the presence of both (4 0 0) and (1 1 1) preferential orientations to the growth conditions, e.g. substrate temperature, the distance between the substrate and the target. In this work, (1 1 1) plane was observed only for SnSe thin films deposited from Sn enriched SnSe precursor at 820 K (cf. Fig. 2a). Analyzing the XRD data of all samples with a database (JCPDS: 01-089-0233) showed that all films have an orthorhombic structure. In addition to these strong (4 0 0) and (1 1 1) peaks, (2 0 0),

Table 2
Structural parameters of SnSe films. (*hkl*)- Miller indices, *d*-the distance between the planes.

T_s (K)	SnSe thin films deposited from Sn enriched SnSe precursor				SnSe thin films deposited from stoichiometric SnSe precursor				SnSe thin films deposited from Se enriched SnSe precursor			
	Composition of the film	2θ (°)	(*h k l*)	*d* (Å)	Composition of the film	2θ (°)	(*h k l*)	*d* (Å)	Composition of the film	2θ (°)	(*h k l*)	*d* (Å)
720	$Sn_{0.55}Se_{0.45}$	25.3	(2 0 1)	3.72	$Sn_{0.48}Se_{0.52}$	15.44	(2 0 0)	5.74	$Sn_{0.48}Se_{0.52}$	15.40	(2 0 0)	5.74
		30.41	(1 1 1)	2.93		30.47	(1 1 1)	2.93		31.07	(4 0 0)	2.87
		31.02	(4 0 0)	2.88		31.11	(4 0 0)	2.87		64.7	(8 0 0)	1.44
		37.95	(0 2 0)	1.92		47.42	(6 0 0)	1.92				
		43.25	(6 1 0)	1.44		64.82	(8 0 0)	1.44				
		64.64	(8 0 0)	1.23								
770	$Sn_{0.5}Se_{0.5}$	15.38	(2 0 0)	5.76	$Sn_{0.48}Se_{0.52}$	15.45	(2 0 0)	5.73	$Sn_{0.49}Se_{0.51}$	15.40	(2 0 0)	5.75
		30.43	(1 1 1)	2.93		30.46	(1 1 1)	2.93		31.07	(4 0 0)	2.87
		31.03	(4 0 0)	2.88		31.10	(4 0 0)	2.87		64.7	(8 0 0)	1.43
		47.31	(6 0 0)	1.92		47.39	(6 0 0)	1.92				
		64.68	(8 0 0)	1.44		64.78	(8 0 0)	1.44				
820	$Sn_{0.55}Se_{0.45}$	21.42	(1 0 1)	4.15	$Sn_{0.49}Se_{0.51}$	15.44	(2 0 0)	5.73	$Sn_{0.49}Se_{0.51}$	15.40	(2 0 0)	5.74
		25.3	(2 0 1)	3.52		30.48	(1 1 1)	2.93		31.08	(4 0 0)	2.87
		29.41	(0 1 1)	3.03		31.11	(4 0 0)	2.87		64.78	(8 0 0)	1.44
		30.44	(1 1 1)	2.93		47.40	(6 0 0)	1.92				
		31.06	(4 0 0)	2.88		64.79	(8 0 0)	1.44				
		37.76	(4 1 0)	2.38								
		43.38	(0 2 0)	2.08								
		49.67	(5 1 1)	1.83								
		64.75	(8 0 0)	1.44								

(2 0 1), (1 1 1), (4 1 0), (4 1 1), (6 0 0), (1 0 1), (0 1 1), (4 0 0), (0 2 0), (5 1 1), and (8 0 0) small peaks are also present, although their intensity was extremely small compared to the intensities of the (4 0 0) and (1 1 1) peaks.

The lattice parameters of the crystal for all samples were calculated using the following formula: $1/d^2 = h^2/a^2 + k^2/b^2 + l^2/c^2$, where d is the distance between the planes, h, k, l are Miller indices and a, b, c are lattice constants. The lattice constants for thin films deposited at different substrate temperatures from Sn and Se enriched and stoichiometric SnSe precursors have the following values: $a = 11.52$ Å, $b = 4.16$ Å, $c = 4.43$ Å and $a = 11.48$ Å, $b = 4.17$ Å, $c = 4.39$ Å, respectively. These values are in good agreement with the JCPDS database, as well as the data presented in the literature for SnSe thin films grown by various methods (Butt et al., 2012; Mathews, 2012). Detailed structural parameters of all films are presented in Table 2.

Fig. 3 illustrates SEM images for all samples grown at different substrate temperatures from Sn and Se enriched as well as stoichiometric SnSe precursors. Although the microcrystals for all SnSe films are uniformly distributed over the film surface, the microstructure (shape and grain size) of the samples depends on both the substrate temperature and the precursor composition. With increasing the substrate temperature, the shape of the grains changes, whereas the grain sizes do not change significantly for the films deposited from Sn enriched SnSe precursor (cf. Fig. 3a), and vice versa for the samples obtained from Se enriched and stoichiometric SnSe precursors (cf. Fig. 3b,c). Furthermore, the grain shapes of all the samples have a flattened appearance for all substrate temperatures, except for films obtained from Sn enriched SnSe compound at a substrate temperature of 820 K, which has the form of a parallelepiped. The samples obtained from Sn enriched precursor have similar grain sizes of (8–10) μm and have a polycrystalline structure for all substrate temperatures. However, the grain sizes of the films deposited from Se enriched and stoichiometric SnSe precursors increased, i.e. (8–20) μm, at the substrate temperature of 820 K and the structure become more densely packed. Moreover, disappearance of vertically deposited grains on the surface of all SnSe films was observed with increasing the substrate temperature.

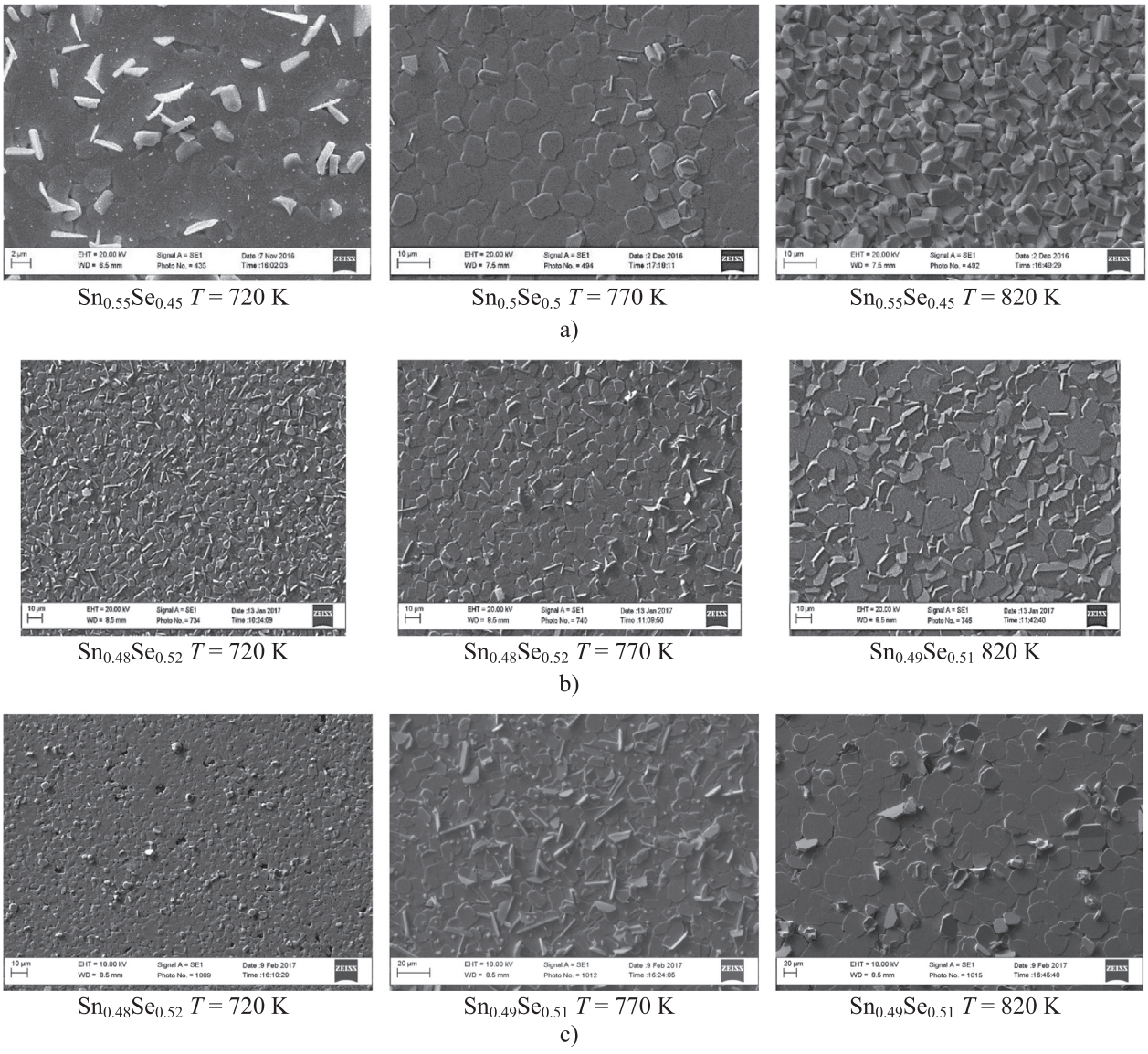

Fig. 3. SEM images of SnSe thin films deposited from (a) Sn enriched, (b) stoichiometric and (c) Se enriched SnSe precursors at indicated substrate temperatures.

Table 3
Electrical parameters of SnSe films. T_s -substrate temperature, σ-electrical conductivity, E_{ac}-activation energy. Note that these parameters were estimated by van der Pauw method along the lateral direction of the samples.

T_s (K)	SnSe thin films deposited from Sn enriched SnSe precursor				SnSe thin films deposited from stoichiometric SnSe precursor				SnSe thin films deposited from Se enriched SnSe precursor			
	Composition of the film	σ (Ohm·cm)$^{-1}$	E_{ac} (eV)	Type of cunductivity	Composition of the film	σ (Ohm·cm)$^{-1}$	E_{ac} (eV)	Type of cunductivity	Composition of the film	σ (Ohm·cm)$^{-1}$	E_{ac} (eV)	Type of cunductivity
720	$Sn_{0,55}Se_{0.45}$	90	0.0023	*p*	$Sn_{0,48}Se_{0,52}$	6,5	0.0023	*p*	$Sn_{0,48}Se_{0,52}$	5,5	0.0022	*p*
770	$Sn_{0,5}Se_{0.5}$	70	0.0024	*p*	$Sn_{0,48}Se_{0,52}$	24	0.0025	*p*	$Sn_{0,49}Se_{0,51}$	20	0.0024	*p*
820	$Sn_{0,55}Se_{0.45}$	15	0.0406	*p*	$Sn_{0,49}Se_{0,51}$	27	0.0026	*p*	$Sn_{0,49}Se_{0,51}$	24	0.0028	*p*

The same results were also reported in (Boscher et al., 2008).

The electrical parameters of the SnSe films, e.g. conductivity σ, activation energy E_{ac} and the type of conductivity, are given in Table 3. As shown, all SnSe thin films exhibit *p*-type conductivity. The electrical conductivity of SnSe films deposited from Sn enriched SnSe precursor decreases with increasing the substrate temperature. This is explained by the increase of Sn content in the film deposited at high substrate temperature. Unlike, the electrical conductivity of those samples obtained from Se enriched and stoichiometric SnSe precursors increases with increasing the substrate temperature. This improvement is associated with an increase in the grain size and a decrease in the grain boundary density of the films grown at higher substrate temperatures (Shikha et al., 2017).

Fig. 4 shows Tauc plot, i.e. $(\alpha h\nu)^2$ vs $(h\nu)$, for selected SnSe thin films with different composition grown at 670 K and 720 K. As shown, the optical bandgap of SnSe thin films has been determined to be in the range of (1.1–1.2) eV in the Tauc plot using linear extrapolation of the leading edge. Since the plot of $(\alpha h\nu)^2$ vs $(h\nu)$ is almost linear, the direct nature of the optical transition in SnSe is confirmed. These obtained values are suitable for photovoltaic application and in good agreement with the reported data of those SnSe films prepared by various growth methods (Indirajith et al., 2010; Butt et al., 2012).

4. Conclusion

We have investigated the morphological, structural, optical and electrical properties of SnSe films for different substrate temperatures and composition.

It has been found that: (1) at low substrate temperatures, SnSe thin films tend to be Se enriched, i.e. more visible in the films grown from stoichiometric and Sn enriched SnSe precursors; (2) with increasing the substrate temperature, foreign particles disappear from the film surfaces and the films have more closely packed polycrystalline structure; (3) the films have an orthorhombic structure and are characterised by preferential (4 0 0) and (1 1 1) plane orientations; (4) the electrical conductivity of the SnSe films deposited from Sn enriched precursor decreases with increasing the substrate temperature, whereas it increases in SnSe films obtained from the Se enriched and stoichiometric SnSe precursors. Further, optical measurements showed that all the SnSe thin films have a bandgap of (1.1–1.2) eV, which is suitable for photovoltaic application.

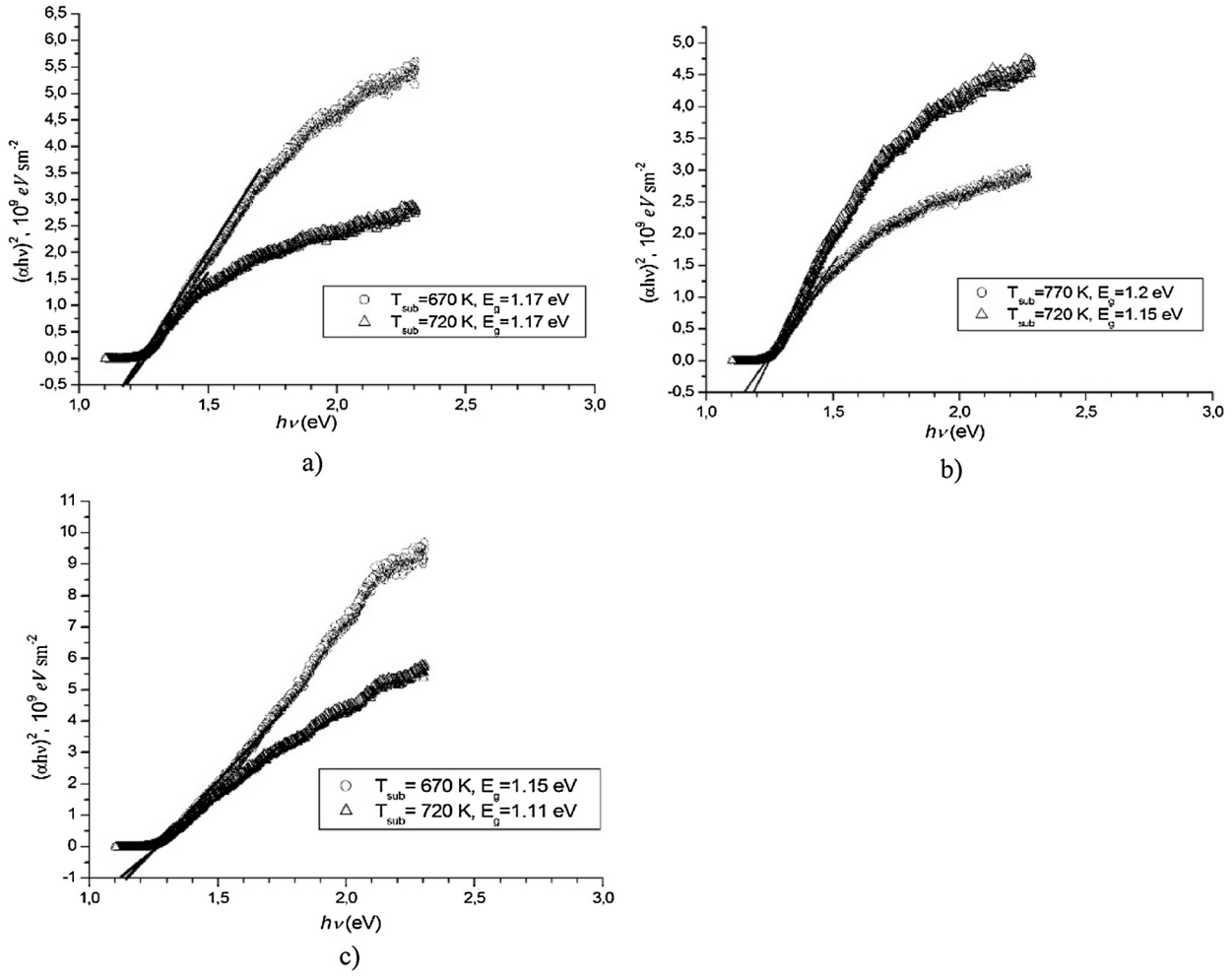

Fig. 4. Absorption coefficient versus photon energy for SnSe thin films deposited from (a) Sn enriched, (b) stoichiometric and (c) Se enriched SnSe precursors at two different substrate temperatures of 670 K and 720 K.

Acknowledgement

The work was carried out within the framework of Fund for Supporting the Fundamental Research (Grant No. F.2-16) and Fundamental Research Project (Grant No. FA-F3-003).

References

Banu, S., Ahn, S.J., Eo, Y.J., Gwak, J., Cho, A., 2017. Tin monosulfide (SnS) thin films grown by liquid-phase deposition. Sol. Energy 145, 33–41.

Boscher, N.D., Carmalt, C.J., Palgrave, R.G., Parkin, I.P., 2008. Atmospheric pressure chemical vapour deposition of SnSe and $SnSe_2$ thin films on glass. Thin Solid Films 516, 4750–4757.

Butt, F.K., Cao, C.B., Khan, W.S., Ali, Z., Ahmed, R., Idrees, F., Aslam, I., Tanveer, M., Li, J., Zaman, S., Mahmood, T., 2012. Synthesis of highly pure single crystalline SnSe nanostructures by thermal evaporation and condensation route. Mater. Chem. Phys. 137 (2), 565–570.

Dhere, N.G., 2011. Scale-up issues of CIGS thin film PV modules. Sol. Energy Mater. Sol. Cells 95 (1), 277–280.

Green, M.A., Emery, K., Hishikawa, Y., Warta, W., Dunlop, E.D., 2016. Solar cell efficiency tables (version 48). Prog. Photovolt: Res. Appl. 24, 905–913.

Hamakawa, Y., 2004. Background and motivation for thin-film solar-cell development. In: Hamakawa, Y. (Ed.), Thin-Film Solar Cells Next Generation Photovoltaics and Its Applications. Springer, Heidelberg, pp. 1–14.

Indirajith, R., Srinivasan, T.P., Ramamurthi, K., Gopalakrishnan, R., 2010. Synthesis, deposition and characterization of tin selenide thin films by thermal evaporation technique. Curr. Appl Phys. 10, 1402–1406.

Jackson, P., Wuerz, R., Hariskos, D., Lotter, E., Witte, W., Powalla, M., 2016. Effects of heavy alkali elements in Cu(In, Ga)Se2 solar cells with efficiencies up to 22.6%. Phys. Status Solidi RRL 10 (8), 583–586.

Jeong, G., Kim, J., Gunawan, O., Pae, S.R., Kim, S.H., Song, J.Y., Lee, Y.S., Shin, B., 2017. Preparation of single-phase SnSe thin-films and modification of electrical properties via stoichiometry control for photovoltaic application. J. Alloy. Compd. 722, 474–481.

Jung, H.R., Shin, S.W., Suryawanshi, M.P., Yeo, S.J., Yun, J.H., Moon, J.H., Kim, J.H., 2017. Phase evolution pathways of kesterite Cu_2ZnSnS_4 and $Cu_2ZnSnSe_4$ thin films during the annealing of sputtered Cu-Sn-Zn metallic precursors. Sol. Energy 145, 2–12.

Kawano, Y., Kodani, Y., Chantana, J., Minemoto, T., 2016. Effects of Na and secondary phases on physical properties of SnS thin film after sulfurization process. Jpn. J. Appl. Phys. 55, 092301.

Kumar, V., Sinha, A., Farooque, U., 2015. Concentration and temperature dependence of the energy gap in some binary and alloy semiconductors. Infrared Phys. Technol. 69, 222–227.

Martínez-Escobar, D., Ramachandran, M., Sánchez-Juárez, A., Rios, J.S.N., 2013. Optical and electrical properties of $SnSe_2$ and SnSe thin films prepared by spray pyrolysis. Thin Solid Films 535, 390–393.

Mathews, N.R., 2012. Electrodeposited tin selenide thin films for photovoltaic applications. Sol. Energy 86, 1010–1016.

Razykov, T.M., 1991. Chemical molecular beam deposition of II-VI binary and ternary compound films in gas flow. Appl. Surf. Sci. 48/49 (1), 89–92.

Razykov, T.M., Kuchkarov, K.M., 2004. The structural change in CdTe and CdSe thin films in chemical molecular beam deposition. Appl. Solar Energy 4, 63–67.

Razykov, T.M., Ferekides, C.S., Morel, D., Stefanakos, E., Ullal, H.S., Upadhyaya, H.M., 2011. Solar photovoltaic electricity: current status and future prospects. Sol. Energy 85, 1580–1608.

Reddy, V.R.M., Gedi, S., Pejjai, B., Park, C., 2016. Perspectives on SnSe-based thin film solar cells: a comprehensive review. J. Mater. Sci.: Mater. Electron. 27 (6), 5491–5508.

Shikha, D., Mehta, V., Sharma, J., Chauhan, R.P., 2017. Effect of deposition temperature on structural, optical and electrical properties of nanocrystalline SnSe thin films. J Mater Sci: Mater Electron 28, 2487–2493.

Suguna, P., Mangalaraj, D., Narayandass, Sa.K., Meena, P., 1996. Structure, composition, dielectric, and AC conduction studies on tin selenide films. Phys. Stat. Sol. (A) 115,

405–416.
Todorov, T.K., Tang, J., Bag, S., Gunawan, O., Gokmen, T., Zhu, Y., Mitzi, D.B., 2013. Beyond 11% efficiency: characteristics of state-of-the-art Cu2ZnSn(S, Se)2 solar cells. Adv. Energy Mater. 3 (1), 34–38.
Vallat-Sauvain, E., Shah, A., Bailat, J., 2006. Epitaxial thin film crystalline silicon solar cells on low cost silicon carriers. In: Poortmans, J., Arkhipov, V. (Eds.), Thin Film Solar Cells, Fabrication, Characterization and Applications. Wiley, Chichester, pp. 1–32.
Wakeham, S.J., Hawkins, G.J., 2006. Investigation of cadmium alternatives in thin-film coatings. In: Proc. SPIE 6286, Advances in Thin-Film Coatings for Optical Applications III, 62860C.
Wang, W., Winkler, M.T., Gunawan, O., Gokmen, T., Todorov, T.K., Zhu, Y., Mitzi, D.B., 2013. Device characteristics of CZTSSe thin-film solar cells with 12.6% efficiency. Adv. Energy Mater. 4 (7), 1301465.
Yoshikawa, K., Kawasaki, H., Yoshida, W., Irie, T., Konishi, K., Nakano, K., Uto, T., Adachi, D., Kanematsu, M., Uzu, H., Yamamoto, K., 2017. Silicon heterojunction solar cell with interdigitated back contacts for a photoconversion efficiency over 26%. Nat. Energy 2, 1–8.
Zakutayev, A., 2017. Brief review of emerging photovoltaic absorber materials. Curr. Opin. Green Sustainable Chem. 4, 8–15.